Available at www.sciencedirect.com

ScienceDirect

journal homepage: www.elsevier.com/locate/he

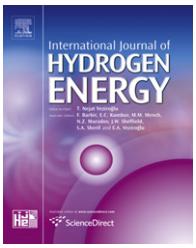

Pd–Ni electrocatalysts for efficient ethanol oxidation reaction in alkaline electrolyte

Zhiyong Zhang [a], *Le Xin* [a], *Kai Sun* [b], *Wenzhen Li* [a,*]

[a] *Department of Chemical Engineering, Michigan Technological University, Houghton, MI 49931, USA*
[b] *Department of Materials Science and Engineering, University of Michigan, Ann Arbor, MI 48109, USA*

ARTICLE INFO

Article history:
Received 29 March 2011
Received in revised form
18 June 2011
Accepted 29 June 2011
Available online 9 August 2011

Keywords:
Electrocatalyst
Nanoparticle
Pd–Ni
Ethanol oxidation
Alkaline
Fuel cell

ABSTRACT

Pd_xNi_y/C catalysts with high ethanol oxidation reaction (EOR) activity in alkaline solution have been prepared through a solution phase-based nanocapsule method. XRD and TEM show Pd_xNi_y nanoparticles with a small average diameter (2.4–3.2 nm) and narrow size distribution (1–6 nm) were homogeneously dispersed on carbon black XC-72 support. The EOR onset potential on Pd_4Ni_5/C (−801 mV *vs.* Hg/HgO) was observed shifted 180 mV more negative than that of Pd/C. Its exchange current density was 33 times higher than that of Pd/C (41.3×10^{-7} A/cm^2 *vs.* 1.24×10^{-7} A/cm^2). After a 10,000-s chronoamperometry test at −0.5 V (*vs* Hg/HgO), the EOR mass activity of Pd_2Ni_3/C survived at 1.71 mA/mg, while that of Pd/C had dropped to 0, indicating Pd_xNi_y/C catalysts have a better 'detoxification' ability for EOR than Pd/C. We propose that surface Ni could promote refreshing Pd active sites, thus enhancing the overall ethanol oxidation kinetics. The nanocapsule method is able to not only control over the diameter and size distribution of Pd–Ni particles, but also facilitate the formation of more efficient contacts between Pd and Ni on the catalyst surface, which is the key to improving the EOR activity.

1. Introduction

Low Temperature hydrogen fueled proton exchange membrane fuel cells (PEMFCs) have recently attracted enormous attention, due to their unique features of high energy conversion efficiency and zero emission [1]. However, the production, transport and storage of hydrogen are facing great technical challenges, and are currently under active research [2]. Lignocellulosic biomass-derived ethanol is considered one of the most promising fuel candidates to substitute H_2 to supply future energy needs [3–5]. Served as a fuel, ethanol has the advantage of reducing CO_2 footprints in the atmosphere because of the absorption of CO_2 by living plant matter that is used as the feedstock to produce it. In 2008, the world bio-ethanol fuel production stood at more than 17 billion US gallons. Blends of gasoline containing 85% denatured ethanol (E85) have recently appeared at fueling stations in the U.S, mainly in the Midwest [6]. However, the efficiencies of heating engines are confined by Carnot cycle limitations (normally < 35%). Direct ethanol fuel cells (DEFCs) are an ideal electrochemical energy device that can directly convert chemical energy of ethanol into electricity without Carnot cycle limitation [2,7–15]. Although DEFCs have a lower theoretical potential (1.15 V *vs.* 1.23 V for H_2-fuel cells at the standard condition) their thermodynamic efficiency of 97% is higher than that for H_2-fuel cells (83%). Ethanol has a volume energy capacity of 6.3 kWh/L, which is higher than hydrogen (2.6 kWh/L) and methanol (4.8 kWh/L). Extensive researches

* *Corresponding author*. Tel.: +1 906 487 2298; fax: +1 906 487 3213.
E-mail address: wzli@mtu.edu (W. Li).

0360-3199/$ – see front matter
doi:10.1016/j.ijhydene.2011.06.141

have been carried out to investigate anode catalysts for proton exchange membrane-based direct ethanol fuel cells (PEM-DEFCs) [7–14]. It has been reported that PtSn-based catalysts have higher activity than other Pt-M (M = Ru, Pd, W, etc) catalysts for ethanol oxidation in acid electrolyte [8–11]. Unfortunately, it was also found that in acid electrolyte, the kinetics of EOR remains sluggish (low activity) and the majority product of EOR is acetic acid (CH_3COOH) not CO_2 (low catalyst selectivity) using PtSn-based catalysts [12,13]. In addition, expensive Pt-based catalysts are required for a long operation life-time in acid electrolytes [1]. The high over potential of oxygen reduction reaction (ORR)–over 200 mV at the most active Pt surface at the cathode–is another long-standing scientific issue to overcome in order to achieve wide applications of PEM-DEFCs [16–19].

Recently, some novel high performance solid anion exchange membranes (AEMs) have been developed and they make alkaline fuel cells more attractive and realistic [15,20–29]. AEMs do not contain mobile metal cations, therefore, they alleviated the fatal issue facing conventional alkaline fuel cells: precipitations of carbonate deteriorating alkaline electrolytes [15]. Direct ethanol anion exchange membrane fuel cells use solid AEM and transform chemical energy stored in ethanol into electrical energy with high efficiency [15,22,28,29]. This is because of: 1) improved kinetics: Slow kinetics of both ethanol oxidation and oxygen reduction reactions can be significantly improved in high pH media, attributed to enhanced ion transport and facile charge transfer [30]; 2) enhanced life-time: non-Pt catalysts can survive in alkali for a longer time than in acid, due to a less corrosive base environment [30]; and 3) reduced cost: non-Pt electrocatalysts have demonstrated high activity to EOR (i.e. Pd, Ni) [31–37] and oxygen reduction reaction (i.e. Ag) [22,23], attributed to enhanced ion transport and mobile charge transfer in alkaline electrolytes [30].

The abundance of Pd on the Earth's crust is 200 times higher than Pt (0.6 ppb vs. 0.003 ppb), the comparatively low price of Pd (only 30%–40% compared to Pt) makes it attractive for large-scale fuel cell applications [38]. Although Pd is nearly inert to EOR in acid electrolytes, it has demonstrated competitive EOR activity [32,37] and slightly better ability to break C–C bond of ethanol in high pH media, as compared to Pt-based catalysts [35]. Pd nanoparticles on hollow carbon, CeO_2/C, and Ni–Zn/C, and PdSn, PdAu, and PdAg alloy nanoparticles have competitive activity as conventional Pt and PtRu electrocatalysts in alkaline electrolyte, but the major products are acetate [31,36,39–41]. It was proposed that adsorbed OH species could facilitate dehydrogenation of ethanol and enhance the EOR on Pd catalysts in high pH media [32]. Density functional theory (DFT) were conducted to calculate the d-band center shift and the segregation energy of transition metals (which occur when two metals are alloyed), and predicted that Pd–Ni had high EOR [42].

It is imperative to develop convenient and efficient synthesis approaches to preparation of Pd-based catalysts with high activity toward ethanol oxidation reaction. In the prior research, Pd-based nanoparticle catalysts were predominantly prepared through aqueous reduction methods, i.e. using $NaBH_4$ as reducing agent [39–41]. However, it is rather difficult to control the particle size and size distribution of metal nanoparticles through aqueous reduction routes. An elegant organic solution phase synthesis approach to self-organized FePt magnetic nanoparticles with controlled assembly thickness and surface roughness was successfully developed by the IBM researchers [43,44]. Later, this method has been extended to prepare carbon supported Pt-M (M = Fe, Co, Ni, Ru, etc), which have been demonstrated high electrocatalytic activity in acid electrolyte, such as oxygen reduction, methanol and formic acid oxidation [45–51].

Recently we modified this solution phase-based nanocapsule method to prepare Pt–Co nanoparticle [52], PtNi@Pt core–shell nanoparticle [53], PdFe nanorod [54], nanoleaves [55] and PtFe nanowires [56] electrocatalysts, and obtained improved electrocatalytic activity to oxygen reduction reaction. In the present article, we modified this method to prepare carbon supported Pd–Ni nanoparticles with different Pd–Ni compositions, and characterized them by XRD, TEM, HR-TEM, TGA, ICP-AES. The characterizations reveal that these Pd–Ni catalysts have small diameters of ~3 nm and narrow size distributions. The catalytic activities toward EOR were measured in 1.0 M NaOH + 1.0 M C_2H_5OH by cyclic voltammetry, linear scan voltammetry, and chonoameperometry. We found the EOR activity is strongly correlated with Pd–Ni composition and structure, especially the interaction and contact between Pd and Ni on the catalyst surface.

2. Experimental section

2.1. Preparation of Pd/C, Pd_xNi_y/C, and Pd_1Ni_1/C–$NaBH_4$ catalysts

The Pd_xNi_y/C catalysts (x:y is the atomic ratio of Pd:Ni) were synthesized through a modified solution phase-based nanocapsule method [51,52,56]. A typical synthesis procedure for the Pd_1Ni_1/C (atomic ratio of Pd:Ni = 1:1) with a Pd loading of ~20 wt % is presented in Scheme 1. In detail, 76.2 mg $Pd(acac)_2$ (0.25 mmol), 73 mg $Ni(acac)_2 \cdot 2H_2O$ (0.25 mmol), and 91 mg Vulcan XC-72R carbon black were mixed in 20 ml benzyl ether solvent, and heated rapidly up to 100 °C under a N_2 blanket. As the temperature increases to 100 °C, 100 μl oleic acid and 100 μl oleylamine were injected into the system, followed by quick injection of 1 ml $LiBet_3H$. The temperature was held for 20 min, and then slowly raised to 180 °C and held for 30 min. The Pd_1Ni_1/C was finally obtained after filtration, washing with copious

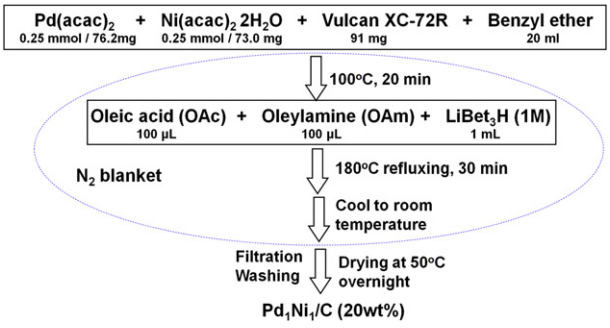

Scheme. 1 – Procedures of nanocapsule synthesis method for preparing Pd_1Ni_1/C catalyst.

ethanol (>800 mL) and drying at 50 °C overnight in an oven. Following a similar procedure, Pd/C and other Pd_xNi_y/C (including Pd_4Ni_1/C, Pd_2Ni_1/C, Pd_4Ni_5/C and Pd_2Ni_3/C) catalysts with the same Pd loading were prepared by adjusting the ratio of metal precursors and the amount of reducing agent ($LiBEt_3H$).

Served as a control sample, Pd_1Ni_1/C catalyst with a Pd loading of ~20% was also synthesized through a widely used $NaBH_4$ reduction method [57–59], which can be described as follows. 44 mg Vulcan 72R carbon black, 28.5 mg $NiCl_2 \cdot 2H_2O$, and 21.3 mg $PdCl_2$ were first dispersed in 100 ml deionized (DI) water under a vigorous stirring. After a homogeneous suspension was formed, 30 ml aqueous solution of $NaBH_4$ (0.02 M) was added into the system dropwisely. The reaction was taken place under a N_2 blanket at room temperature for 24 h. The resulted product was collected by filtration, washing with hot DI water, and drying at 50 °C in an oven, and was named Pd_1Ni_1/C–$NaBH_4$.

2.2. Characterizations

The composition, morphology, and structure of Pd/C and Pd_xNi_y/C catalysts were analyzed by X-ray diffraction (XRD), transmission election microscopy (TEM), High resolution-TEM (HR-TEM), energy dispersive X-ray spectroscopy (EDS), inductively coupled plasma atomic emission spectroscopy (ICP-AES), and thermogravimetric analysis (TGA). XRD patterns were collected by a Scintag XDS-2000 θ/θ diffractometer with Cu K_α radiation ($\lambda = 1.5406$ Å), with a tube current of 35 mA and a tube voltage of 45 kV. TEM was performed by JEOL 2010 with an operating voltage of 200 kV, and HR-TEM was performed on a JEOL 2040 with an operating voltage of 300 kV. 5.0 mg Pd_xNi_y/C catalyst was dissolved in aqua regia (a strong acid mixture with HCl: HNO_3 volume ratio of 3: 1) to form a Pd–Ni aqueous solution, and ICP-AES was performed to detect the concentration of Pd and Ni to obtain the bulk ratio of Pd–Ni and catalyst metal loading. TGA was carried out on TGA Q500 (TA Instruments). The temperature was first increased from room temperature (R.T.) to 500 °C in N_2 at a ramp rate of 20 °C/min. After holding at 500 °C for 10 min, the carrier gas was switched to air and the temperature was further increased to 900 °C at the same ramp rate.

2.3. Electrochemical tests

A conventional three-compartment-cell (AFCELL3, Pine Instrument) with a glassy carbon working electrode (GCE), a Hg/HgO reference electrode, and a Pt wire counter electrode, was used for cyclic voltammetry (CV), linear scan voltammetry (LSV), chronoamperometry (CA) tests of the Pd/C and Pd_xNi_y/C catalysts at room temperature. All potentials in the present study were given *vs.* Hg/HgO (1.0 M NaOH) electrode (0.140 V *vs.* NHE) unless otherwise mentioned [60]. Before each testing, 1.0 mg of the catalyst was first dispersed in 1.0 ml ethanol and ultrasonically-treated for 5 min to make a uniform ink. The working electrode was prepared by dropping 20 μl of the ink on the pre-polished GCE, which was subsequently covered by 10 μl of 0.05 wt% tris(2,4,6-trimethoxyphenyl) polysulfone-methylene quaternary phosphonium hydroxide (TPQPOH) solution [26].

The electrochemical surface areas (ECSAs) of Pd/C and Pd_xNi_y/C catalysts was studied by CV test performed for 20-cycles from −0.87–0.50 V in 1.0 M NaOH with a scan rate of 50 mV/s, and was calculated based on the PdO reduction peak instead of the hydrogen desorption peak, according to our previous publication [55] and Ref [61,62]. The EOR activity was measured by a 20-cycle-CV test from −0.87–0.20 V with the same scan rate. A LSV from −0.87–0.20 V was conducted on each catalyst with a sweep rate of 1 mV/s. The lower potential range (−0.55 to −0.35 V) of LSV was used to obtain the Tafel slope and exchange current density. The onset potential of EOR is defined as the potential where the inflection is observed on the quasi-steady state polarization curve. The long-term activity of EOR was investigated through a chronoamperometry test at an applied voltage of −0.5 V for 10,000 s. The working electrolyte is 1.0 M NaOH + 1.0 M C_2H_5OH.

3. Results and discussion

The bulk chemical compositions of Pd/C, Pd_xNi_y/C, and Pd_1Ni_1/C–$NaBH_4$ catalysts were studied by both ICP-AES and TEM-EDS, as summarized in Table 1. The atomic ratios of Pd:Ni in all the Pd_xNi_y/C catalysts have been determined to be close to the setting ratios, indicating that both Pd and Ni metal precursors have been fully reduced in the synthesis system. The Pd loading of each catalyst has also been calculated through the Pd concentration that was detected by ICP-AES. Because of the existence of small amount of surfactant on the surface of as-prepared catalysts, and the formation of NiO and $Ni(OH)_2$ as the sample is exposed to the air [63], the Pd metal loading of all the catalysts has been found lower than the setting loading of ~20% for all the samples.

Table 1 – Summary of physical properties of Pd/C, Pd_xNi_y/C, and, Pd_1Ni_1/C catalysts.

	Atomic ratio detected by ICP-AES	Pd metal loading detected by ICP-AES	Diameter calculated from XRD (nm)	Lattice parameter calculated from XRD (Å)	Diameter measured by TEM (nm)	Atomic ratio detected by TEM-EDS
Pd/C	–	18%	2.2	3.9207	2.7	–
Pd_4Ni_1/C	$Pd_{7.25}Ni_1$	17%	2.5	3.9080	2.6	$Pd_{5.7}Ni_1$
Pd_2Ni_1/C	$Pd_{1.91}Ni_1$	17%	2.6	3.9078	2.6	$Pd_{2.3}Ni_1$
Pd_1Ni_1/C	$Pd_{1.03}Ni_1$	15%	2.4	3.9102	2.4	$Pd_{0.8}Ni_1$
Pd_4Ni_5/C	$Pd_{3.86}Ni_5$	16%	2.5	3.8950	3.0	$Pd_{3.8}Ni_5$
Pd_2Ni_3/C	$Pd_{1.99}Ni_3$	16%	3.0	3.8900	3.2	$Pd_{1.8}Ni_3$
Pd_1Ni_1/C-$NaBH_4$	$Pd_{1.25}Ni_1$	16%	3.9	3.8930	3.8	$Pd_{1.1}Ni_1$

Fig. 1 shows the TGA curves on Pd/C and Pd_1Ni_1/C catalysts. The temperature-time plots on the two catalysts are identical, as shown in the Fig. 1 inserted. The first two steps were carried out from R. T. to 500 °C in inert N_2 gas, and the third step is from 500 to 700 °C in oxidative air. Due to the oxidation of metal catalysts at high temperature in the air, the metal loadings detected by TGA (22% for Pd/C and 30% for Pd_1Ni_1/C) have been found higher than that determined by IPC-AES. The weight loss at around 100–130 °C in the TGA curve of Pd/C belongs to the evaporation/desorption of water absorbed in the catalyst. The slow weight loss from thereafter to 500 °C is assigned to the gradual decomposition of surfactants in N_2, the surfactants on the Pd/C surface are around 5 wt%. The huge weight loss from 500 to 520 °C is the rapid oxidation of carbon support in air. The presence of $Ni(OH)_2$ is evidenced by the TGA curve of Pd_1Ni_1/C with the weight loss present from 190 to 260 °C, which is attributed to the dehydration of $Ni(OH)_2$, according to the following reaction (1) [64]:

$$Ni(OH)_2 \rightarrow NiO + H_2O \quad (1)$$

The XRD patterns of the Pd/C, Pd_xNi_y/C, and Pd_1Ni_1/C–$NaBH_4$ catalysts are shown in Fig. 2(a) and (b). All of them displayed a typical face-centered cubic (fcc) pattern. The peaks at 39.9°, 45.9°, 67.9°, and 81.8° are assigned to the Pd (111), (200), (220), and (311), respectively, while the peak around 25.2 ° is referred to the graphite (002) facet of Vulcan 72R. The Pd (222) diffraction peak at ~ 86.6 ° has also been observed in Pd_1Ni_1/C-$NaBH_4$ (Fig. 2(b)). In our research, no significant peak shift is observed for the Pd_4Ni_1/C, Pd_2Ni_1/C, and Pd_1Ni_1/C, and only small shifts have been observed for the Pd_4Ni_5/C and Pd_2Ni_3/C (Fig. 2(a)), and Pd_1Ni_1/C-$NaBH_4$ (Fig. 2(b)) catalysts, which suggests that Ni is hard to alloy well with Pd using the presented low reduction temperature. The lattice parameter of the Pd_xNi_y/C catalyst gets smaller (from 3.9080 Å to 3.8900 Å) with Ni amount increasing, as shown in Table 1. Further, the diffraction peaks of Pd_1Ni_1/C–$NaBH_4$ shift more positively than that of Pd_1Ni_1/C (Fig. 2(b)), the Pd_1Ni_1/C-$NaBH_4$ has a lattice parameter of 3.8930 Å, which is smaller than 3.9102 Å for Pd_1Ni_1/C. This indicates that the $NaBH_4$ method

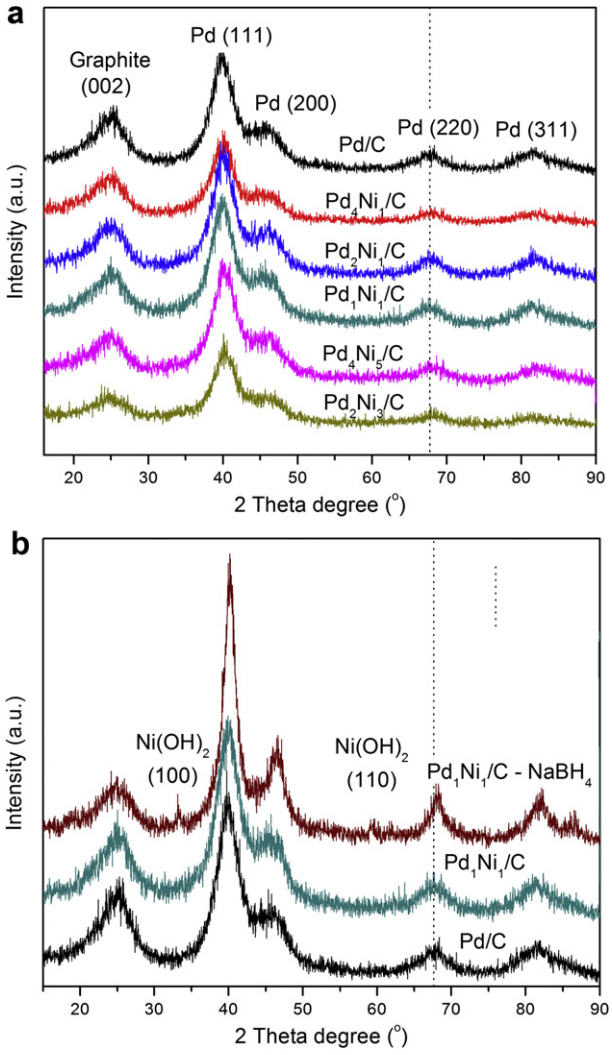

Fig. 2 – XRD patterns of (a) Pd/C and Pd_xNi_y/C catalysts with different Pd:Ni compositions prepared by nanocapsule method; and (b) Pd_1Ni_1/C catalysts prepared by the nanocapsule and $NaBH_4$ reduction methods.

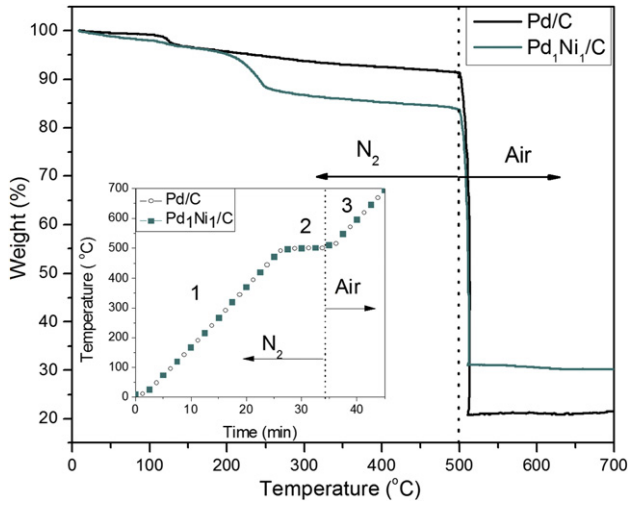

Fig. 1 – Thermogravimetric analysis plot and temperature plot (inserted) of Pd/C and Pd_1Ni_1/C catalysts.

can facilitate the formation of a better Pd–Ni alloy structure. It has been reported that the diffraction peaks shifted to higher 2θ for Pd–Ni catalysts under thermal-treatment at high temperature of over 800 °C [65]. The weak-alloying of Pd and Ni has also been reported for low temperature synthesis of Pd_xNi_y/C catalysts when $NaBH_4$ was introduced as a reducing agent [52–55]. Although Ni will be generally oxidized in air, no diffraction peaks of metallic Ni, Ni oxides and Ni hydroxides were observed for all catalysts prepared by the nanocapsule method, indicating that most of the Ni was amorphous in nature or crystalline only in very small region [63,66]. The XRD pattern of Pd_1Ni_1/C–$NaBH_4$ shows two additional peaks at 33.4° and 59.2°, which are attributed to $Ni(OH)_2$ (100) and (110) facets respectively [57,67,68]. The different XRD patterns in Fig. 1(b) suggests that the presence of H_2O in the $NaBH_4$ reduction process will facilitate the formation of $Ni(OH)_2$ phase. The average particle sizes are calculated based on Pd (220) peak using Debye-Scherrer formula, and are summarized in Table 1. All the Pd/C and Pd_xNi_y/C prepared by the

nanocapsule method have a small particle size in the range of 2.2–3.0 nm, while that of Pd_1Ni_1/C–$NaBH_4$ is 3.9 nm. This strongly suggests the nanocapsule method is more advantageous than traditional $NaBH_4$ method in controlling the particle size.

Fig. 3 shows typical TEM images of the Pd/C, Pd_xNi_y/C, and Pd_1Ni_1/C–$NaBH_4$ catalysts. The average diameters of all the catalysts are summarized in Table 1. They are 2.7, 2.6, 2.6, 2.4, 3.0, 3.2, and 3.8 nm for Pd/C, Pd_4Ni_1/C, Pd_2Ni_1/C, Pd_1Ni_1/C, Pd_4Ni_5/C, Pd_2Ni_3/C, and Pd_1Ni_1/C–$NaBH_4$, respectively. The particle sizes measured from TEM images are in good agreement with those calculated by XRD. All the catalysts prepared by the nanocapsule method are spherical and homogeneously dispersed on Vulcan XC-72R with no remarkable observation of agglomerations. The particle size histograms measured from 100 random particles in an arbitrarily chosen area present a narrow distribution of 1–6 nm for all catalysts prepared by the nanocapsule method. In contrast, the particle size distribution of Pd_1Ni_1/C–$NaBH_4$ is broader (1–9 nm), with some very large particles in TEM image (as shown in Fig. 3(g)). The HR-TEM images of Pd_1Ni_1/C and Pd_1Ni_1/C–$NaBH_4$ are shown in Fig. 4. It is clearly observed that Pd_1Ni_1/C has a smaller particle size than Pd_1Ni_1/C–$NaBH_4$. Further, the HR-TEM images show that both two catalysts have same type of lattice fringe with an interplanar spacing of ~0.24 nm, indicating that they are covered by the Pd (111) plane.

The cyclic voltammograms of Pd/C, Pd_xNi_y/C, and Pd_1Ni_1/C–$NaBH_4$ catalysts were investigated in 1.0 M NaOH solution and are shown in Fig. 5(a) and (b). The CV curves clearly show that both Pd and Ni are present on all Pd_xNi_y/C and Pd_1Ni_1/C–$NaBH_4$ catalysts. On the pure Pd/C polarization curve, a small peak at ~–0.3 V is ascribed to the water activation on Pd [66]. However, when combined with Ni, this peak was suppressed and a broad peak at ~–0.53 V appeared instead, which can be assigned to the OH^- adsorption on the surface of the Pd_xNi_y/C catalysts. The presence of both Pd and Ni in the Pd_xNi_y/C and Pd_2Ni_3/C–$NaBH_4$ catalysts can also been confirmed by the oxidation peak of $Ni(OH)_2$ to NiOOH in the anodic sweep at the region of 0.4–0.5 V, and the reduction of NiOOH to $Ni(OH)_2$ in the cathodic sweep at the region of 0.2–0.5 V [66,69,70], and the reduction of PdO to Pd at around –0.3 V [71,72]. Due to the penetration of hydrogen into the Pd and Pd-based bimetallic nanostructures, the ECSAs of the Pd, Pd_xNi_y/C, and Pd_1Ni_1/C–$NaBH_4$ catalysts were calculated by the charge of the reduction region of PdO to Pd, and are summarized in Table 2. Although Pd_4Ni_1/C, Pd_2Ni_1/C, and Pd_1Ni_1/C catalysts possesses high ECSAs as the result of their small particle sizes, a trend of decrease in ECSA has been

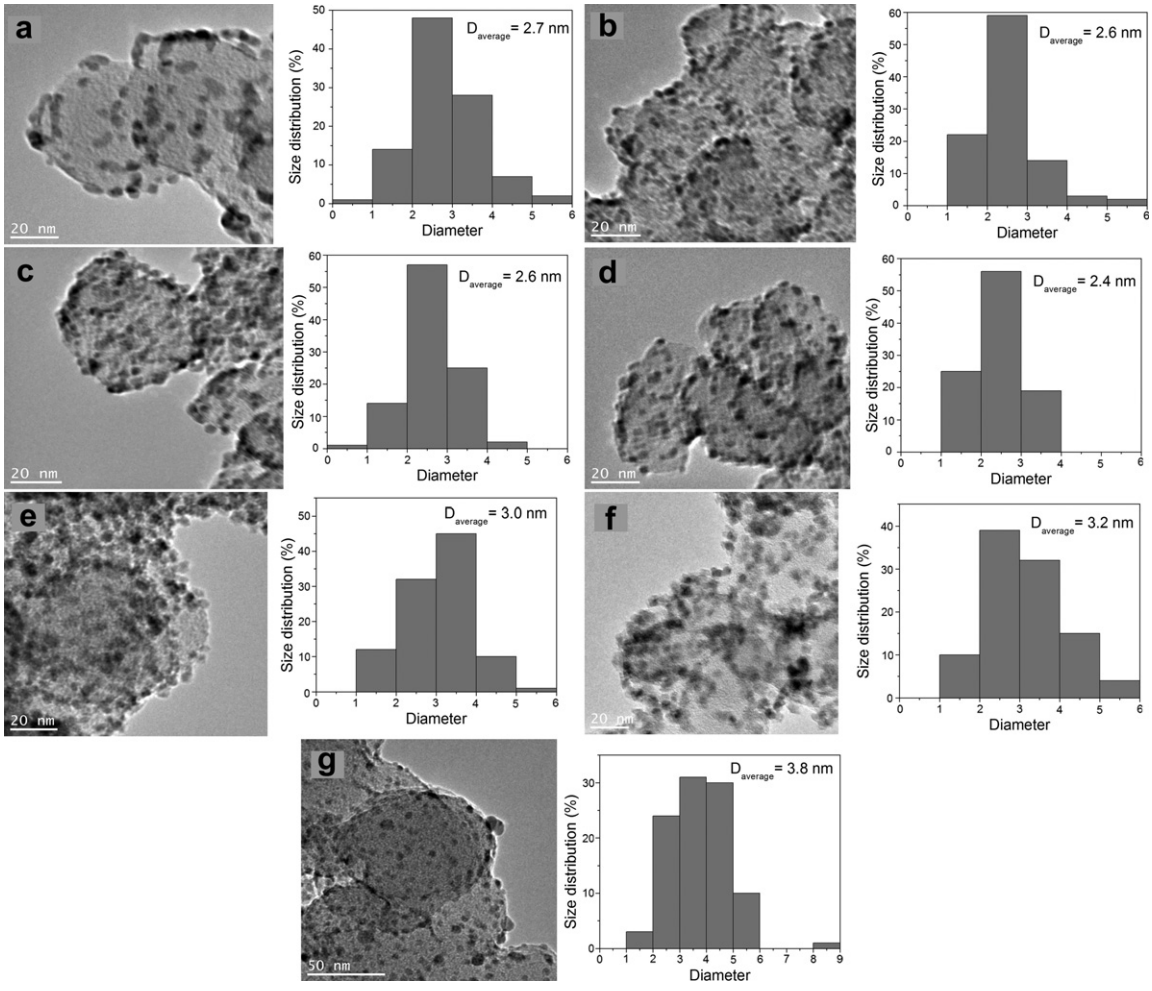

Fig. 3 – TEM images of and particle size histograms (a) Pd/C, (b) Pd_4Ni_1/C, (c) Pd_2Ni_1/C, (d) Pd_1Ni_1/C, (e) Pd_4Ni_5/C, (f) Pd_2Ni_3/C, and (g) Pd_1Ni_1/C-$NaBH_4$ catalysts.

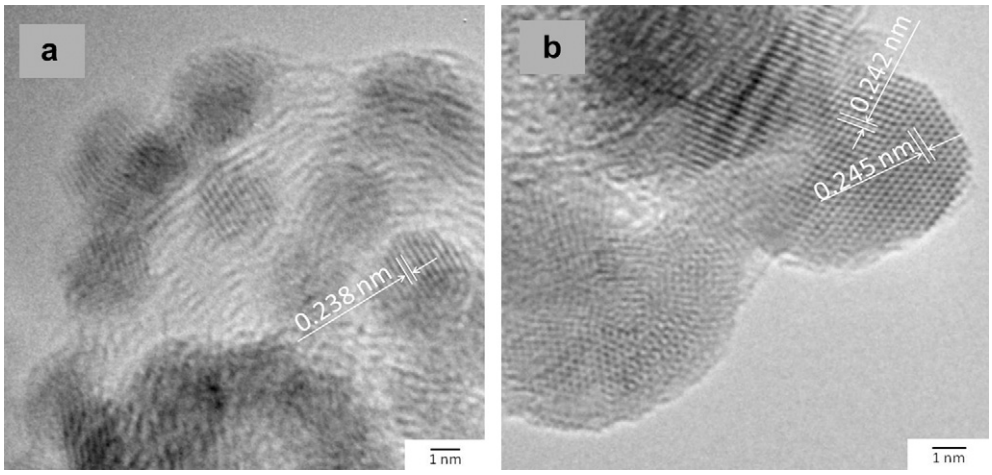

Fig. 4 – HR-TEM images of (a) Pd_1Ni_1/C and (b) Pd_1Ni_1/C-$NaBH_4$, both showing Pd (111)-rich surface.

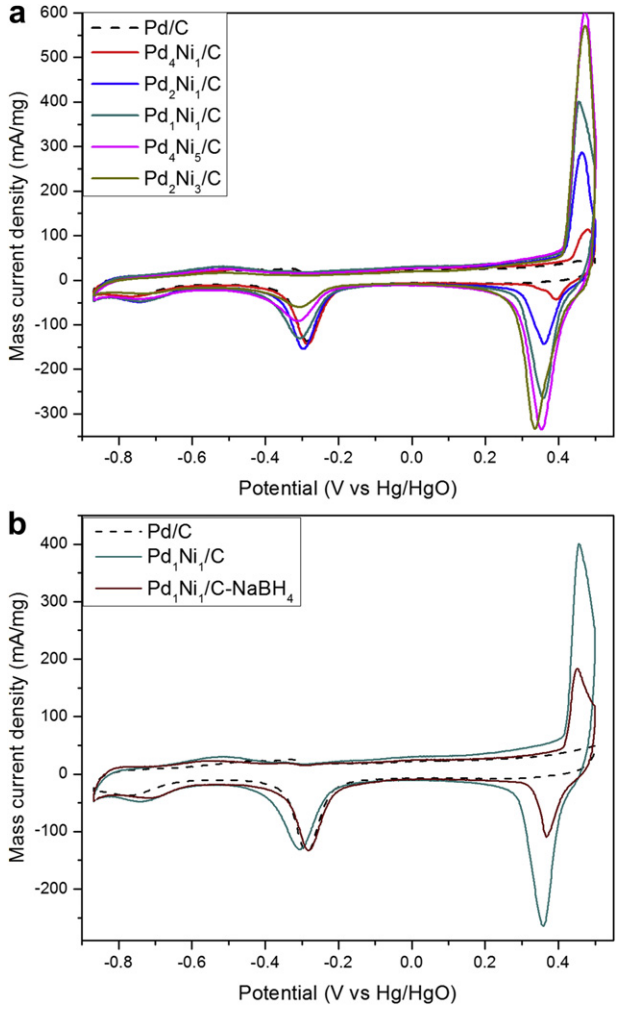

Fig. 5 – Cyclic voltammograms of (a) Pd/C and Pd_xNi_y/C catalysts prepared by the nanocapsule method and (b) Pd/C, Pd_1Ni_1/C, and Pd_1Ni_1/C-$NaBH_4$ catalysts in 1.0 M NaOH, at 50 mV/s, room temperature.

found on the Pd_xNi_y/C with a high Ni concentration. Because Pd and Ni could not alloy well using the nanocapsule method, this decrease may be a clue that portion of the surface Pd active sites were covered by excessive Ni or Ni derivatives. The Ni-rich surface on the nanocapsule-synthesized Pd_xNi_y/C catalysts was more obvious when comparing the CV curves of Pd_1Ni_1/C and Pd_1Ni_1/C–$NaBH_4$. Although the HR-TEM images clearly show that the two catalysts have same Pd (111) surface plane, the CV curve of Pd_1Ni_1/C presents a pair of $Ni(OH)_2$–NiOOH oxidation-reduction peaks, which are much larger than that of Pd_1Ni_1/C–$NaBH_4$ (as shown in Fig. 5(b)). This implies that even with the same bulk Pd–Ni atomic ratio, more Ni is located on the surface of nanocapsule-synthesized Pd_1Ni_1/C catalyst. This is consistent with the XRD results. With a better alloy structure, Pd_1Ni_1/C–$NaBH_4$ has more Ni inserted into Pd lattice, leading to a relatively less amount of Ni remaining on the surface. As the benefit of small diameter, the nanocapsule method synthesized Pd_1Ni_1/C catalyst has a larger electrochemical surface area (ECSA) than Pd_1Ni_1/C–$NaBH_4$, therefore, it has more Pd active sites.

The EOR curves on the Pd/C, Pd_xNi_y/C, and Pd_1Ni_1/C–$NaBH_4$ catalysts are presented in Fig. 6(a) and (b), and they are all characterized by two well-defined peaks, designated as Peak I, centered at ~−0.08 V in the anodic sweep curve, and Peak II, centered at ~−0.17 V in the cathodic sweep curve. The mass activities (MAs) of Pd/C, Pd_xNi_y/C, and Pd_1Ni_1/C-$NaBH_4$ catalysts at −0.5 V and their corresponding specific activities (SAs) are summarized in Table 2.

Based on the previous study, the mechanism of EOR on Pd can be described through the follow Eqs. (2)–(5) [73–75]:

$$Pd + CH_3CH_2OH \leftrightarrow Pd - (CH_3CH_2OH)_{ads} \quad (2)$$

$$Pd - (CH_3CH_2OH)_{ads} + 3OH^- \rightarrow Pd - (CH_3CO)_{ads} + 3H_2O + 3e^- \quad (3)$$

$$Pd - (CH_3CO)_{ads} + Pd - OH_{ads} \xrightarrow{r.d.s} Pd - CH_3COOH + Pd \quad (4)$$

$$Pd - CH_3COOH + OH^- \rightarrow Pd + CH_3COO^- + H_2O \quad (5)$$

Reaction (1) and (2) are generally accepted to happen at a potential region of <−0.7 V in the anodic sweep. The

Table 2 – Electrochemical surface area (ECSA), EOR mass activity and specific activity on Pd/C, Pd_xNi_y/C, and, Pd_1Ni_1/C catalysts.

	ECSA (m^2/g)	Mass activity at Peak I at 50 mV/s (mA/mg_{Pd})	Specific activity at Peak I at 50 mV/s (A/m^2)	Mass activity at Peak I at 1 mV/s (mA/mg_{Pd})	Specific activity at Peak I at 1 mV/s (A/m^2)
Pd/C	58.0	2831.74	48.80	729.62	12.57
Pd_4Ni_1/C	63.8	2779.80	43.59	906.59	14.22
Pd_2Ni_1/C	68.0	2956.62	43.50	1197.24	17.61
Pd_1Ni_1/C	67.3	2368.22	35.18	1247.51	18.53
Pd_4Ni_5/C	48.3	856.79	17.76	444.88	9.22
Pd_2Ni_3/C	32.9	544.22	16.56	315.62	9.60
Pd_1Ni_1/C-$NaBH_4$	58.1	1938.43	33.34	960.37	16.52

CH_3CO_{ads} or other carbonaceous reactive intermediates will strongly absorb on the surface of Pd and block the active sites. Reactions (3) and (4) take place in the region starting from −0.7 V, where Pd begins to adsorb OH^-. With the adsorption of hydroxyl on Pd, the strongly absorbed carbonaceous species will be quickly stripped away, and result in an increasing current. However, at a higher potential, the formation of PdO will block further adsorption of reactive species and lead to a remarkable decrease in current [35,74,76]. In the cathodic sweep, the previously formed PdO will be reduced to catalytic active Pd, thus, leading to the recovery of EOR current. Although peak II is assigned by some authors to the removal of carbonaceous species that are not completely oxidized in the anodic scan [39,77], no solid evidence has ever been reported to support their proposed mechanism that the intermediates generated in the forward scan will strongly bond on the surface of PdO in alkaline solution in high-potential range. Therefore, it is reasonable to believe these intermediates should diffuse into the bulk electrolyte. When PdO was reduced back to Pd, the newly-produced catalytic surface should be directly exposed to fresh ethanol. The high-potential and the quick adsorption of OH^- will benefit the generation of high current density and lead to a sharp anodic peak.

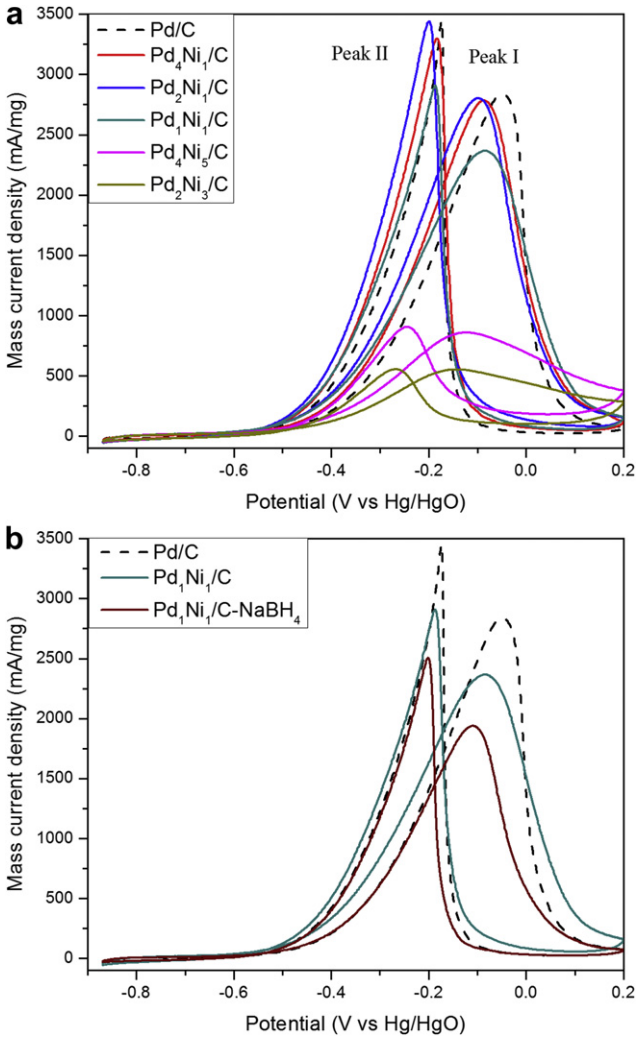

Fig. 6 – Cyclic voltammograms of (a) Pd/C and Pd_xNi_y/C prepared by the nanocapsule method and (b) Pd/C, Pd_1Ni_1/C, and Pd_1Ni_1/C–$NaBH_4$ catalysts in 1.0 M NaOH + 1.0 M C_2H_5OH, 50 mV/s, room temperature.

As could be seen in Eq. (3), ethanol oxidation is determined by the degree of coverage of both CH_3CO_{ads} and OH_{ads}. Therefore, when Ni is involved, the formed $Ni(OH)_2$ on the surface of Pd-based catalysts will facilitate the ethanol oxidation by increasing OH at lower potential range species, and result in the decrease of onset potential, as shown in Fig. 5(a). However, it is interesting to observe that as the Ni amount increases, the specific activity (SA) at Peak I reduces monotonically from 48.80 A/m^2 for Pd/C to 16.56 A/m^2 for Pd_2Ni_3/C. This degradation may rise from two possible reasons. First, $Ni(OH)_2$ formed during the test will increase the concentration of OH^- and/or OH_{ads}. If the concentration is too high, it will reduce/block the transportation of ethanol to Pd active sites, leading to the reduction of Pd–CH_3CO_{ads}. Second, more Ni was covered on the surface of the nanocapsule-synthesized Pd_xNi_y/C catalysts, if Ni is in excess, it will block the Pd active sites, thus reducing the overall EOR catalytic activity.

When compared to traditional $NaBH_4$ reduction method, the present nanocapsule method shows a great advantage in improving the EOR activity, which can be seen in Fig. 4(b) and Table 2. The nanocapsule-synthesized Pd_1Ni_1/C possesses both a lower onset potential and higher SA. Since the HR-TEM images in Fig. 4 present that both Pd_1Ni_1/C and Pd_1Ni_1/C–$NaBH_4$ have the same Pd (111) surface, the geometric effects can be neglected. The main reason for the EOR enhancement on Pd_1Ni_1/C lies in a special Pd–Ni synergistic effect, which is originated from the better contacts or more efficient co-operation between Pd and Ni on the catalyst

surface. Moreover, due to the small particle size and narrow size distribution, the MA of Pd_1Ni_1/C can reach 2368.22 mA/mg_{Pd}, which is 429.79 mA/mg_{Pd} higher than the corresponding $NaBH_4$-reduced catalyst (1938.43 mA/mg_{Pd}). It needs to mention that the MAs of both the Pd_1Ni_1/C and Pd_1Ni_1/C–$NaBH_4$ reported in this study are higher than that of previously reported Pd–Ni/C (1136.13 mA/mg_{Pd}) under identical test conditions [57]. The MAs of our nanocapsule-synthesized Pd_4Ni_1/C, Pd_2Ni_1/C and Pd_1Ni_1/C catalysts are also higher than other reported results on Pd-based catalysts [32,78–81]. Since the Pd_1Ni_1/C–$NaBH_4$ was prepared by a surfactant-free method, the surface of catalysts is clean. Thus, this catalyst has very little surfactant effects. Our results indicate that small amount of surfactants (OAc and OAm, around 5 wt% determined by TGA) on Pd_xNi_y/C will not apparently affect the EOR activities.

To further study the EOR mechanism, a conventional linear scan voltammogram of EOR has been carried out on Pd/C, Pd_xNi_y/C, Pd_1Ni_1/C–$NaBH_4$ catalysts at a sweep rate of 1 mV/s in 1.0 M NaOH + 1.0 M C_2H_5OH, and the results are shown in Fig. 7. It is reasonable to consider the ethanol oxidation reaction taking place on catalysts in such slow sweep rate to be at quasi-steady state, therefore, this method minimizes the mass transfer/diffusion issues. The MA and SA at the peak current of EOR at quasi-steady state are summarized in Table 2. The data show that the addition of Ni at a certain content can significantly increase the EOR activity on Pd, while too much of Ni will cause the drop of EOR activity. The surface concentration of Ni also significantly affects the onset potentials. As shown in Table 3, the lowest onset potential of −801 mV has been achieved on Pd_4Ni_5/C, which is 180 mV more negative than that of Pd/C. In light of XRD and TEM analysis, the discrepancies of Pd and Pd_xNi_y metal particle size and distributions on carbon black support were rather small and contributed little to the enhanced EOR activity. The changes in catalytic activity and onset potential mainly rely on the synergistic effect between Pd and Ni. The major existing Ni species during the test is $Ni(OH)_2$, which has a point of zero charge (PZC) varying from pH = 8.8 ~ 11

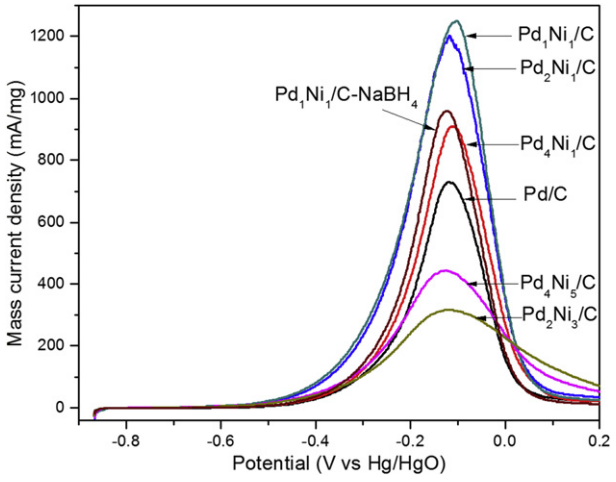

Fig. 7 – Quasi-steady state linear scan voltammograms of Pd/C and Pd_xNi_y/C and Pd_1Ni_1/C–$NaBH_4$ catalysts 1.0 M NaOH + 1.0 M C_2H_5OH, at 1.0 mV/s, room temperature.

Table 3 – Onset potential, Tafel slope and exchange current density of EOR on the Pd/C, Pd_xNi_y/C, and, Pd_1Ni_1/C catalysts (at room temperature).

	Onset potential (mV)	Tafel slope (V/dec)	Exchange current density ($\times 10^{-7}$ A/cm^2)
Pd/C	−621	0.128	1.24
Pd_4Ni_1/C	−718	0.157	5.87
Pd_2Ni_1/C	−758	0.171	22.4
Pd_1Ni_1/C	−769	0.170	22.5
Pd_4Ni_5/C	−801	0.206	41.3
Pd_2Ni_3/C	−750	0.210	39.8
Pd_1Ni_1/C-$NaBH_4$	−669	0.139	2.57

[82–84]. Therefore, $Ni(OH)_2$ in 1.0 M NaOH solution would absorb OH^- and increase the OH^- local concentration around the catalysts nanoparticles. The raise of local OH^- concentration will further lead to the enhancement of OH_{ads}, which is evidenced by the broad peak on Pd_xNi_y/C catalysts in Fig. 5 (a), centered at ~−0.53 V. As mentioned before, the ethanol oxidation is related with both CH_3CO_{ads} and OH_{ads}. The addition of Ni on surface will increase the coverage of OH_{ads} and accelerate the reaction rate to some extent. Since the adsorption of OH^- on pure Pd in alkaline electrolyte is generally accepted to from −0.7 V vs Hg/HgO electrode, the EOR onset potential of −0.621 V on the Pd/C catalyst is a little above −0.7 V, indicating that a certain amount of OH_{ads} coverage is essential to generate detectable current density. The addition of Ni will enhance the generation of OH_{ads} at relatively negative potential, and therefore lower the onset potential of EOR. On the other hand, Eq. (3) indicates that the CH_3CO_{ads} 'poison' or other intermediates can be removed by increasing the concentration of OH_{ads}. Thus, Ni will also serve to promote refreshing Pd active sites, thus improving the overall reaction rate. Based on the above discussion, Eq. (4) on Pd_xNi_y/C catalysts can be rewritten as Eq. (6):

$$Pd-(CH_3CO)_{ads}+OH^- \xrightarrow{Ni(OH)_2} Pd-CH_3COOH+e^- \quad (6)$$

As discussed in the CV performance in 1.0 M NaOH solution, Ni species are more likely to be rich at the surface of nanocapsule-synthesized Pd_xNi_y/C catalysts. Too much Ni will lead to the blockage of Pd active sites. Previous work by other groups has already demonstrated that Ni itself has no activity toward ethanol oxidation in alkaline solution in the potential range we investigated in this study [63]. Too much Ni will reduce both the onset potential and MA due to the lack of Pd active sites. At the same time, excessive amount of Ni will increase the coverage of OH_{ads} so much that the whole reaction is retarded by the insufficient supply of CH_3CO_{ads}. In this research, the lowest onset potential and the largest MA have been found on Pd_4Ni_5/C and Pd_1Ni_1/C, respectively, indicating more efficient contacts or interactions between Pd and Ni species can be created through the present nanocapsule method.

To the purpose of comparing the kinetic activities of Pd/C, Pd_xNi_y/C, and Pd_1Ni_1/C–$NaBH_4$ catalysts toward EOR, Tafel polarization analysis of Pd_xNi_y/C catalysts was provided and the results are shown in Table 3. The relationship between the current density and over potential is described as Eq. (7):

$$\eta = 2.303\frac{RT}{\alpha nF}\log\left(\frac{j}{j_0}\right) \quad (7)$$

where η is the over potential (η = E-E_{theory}), α is the anodic transfer coefficient, n is the number of electrons transferred in the reaction, j_0 is the exchange current density. E_{theory} is set as 0.10 V vs NHE, which represents the potential of oxidation of ethanol to carbon dioxide [85, 86]. Taking into the consideration of the pH effect (Eq. (8)) and potential shift between Hg/HgO and NHE in 1.0 M NaOH solution, which is 0.140 V [60], E_{theory} is calculated to be ~−0.87 V vs. Hg/HgO electrode.

$$E = E^0 + \frac{RT}{F}\ln\ a_{H^+} \quad (8)$$

The quantity proceeding the logarithm is defined as Tafel slope $b = 2.303RT/\alpha nF$, the Tafel slope given was derived in the low potential range of −0.55 to −0.35 V by plotting the over potential, η, against the logarithm of current density. It is reported that within such potential range, the adsorption of CH_3CO_{ad} is independent of the potential (Eq. (2)) and the kinetics of EOR is determined by the adsorption of OH^- on the electrode surface [74]. The exchange current density j_0 was obtained by extrapolating the linear fitted Tafel line to where the over potential equals zero. The results summarized in Table 3 show the exchange current density toward EOR on Pd/C and Pd_xNi_y/C catalysts follows the same trend of onset potential, with the highest exchange current density achieved on Pd_4Ni_5/C of 41.3 × 10^{-7} A/cm^2, which is 33 times higher than that of Pd/C (1.24 × 10^{-7} A/cm^2). The exchange current density on Pd_1Ni_1/C (22.5 × 10^{-7} A/cm^2) is 18 times and 9 times higher than that of Pd/C and Pd_1Ni_1/C–$NaBH_4$, respectively, indicating that a more efficient catalyst can be prepared through the nanocapsule method.

The long-term reactivity of EOR on Pd/C, Pd_xNi_y/C, and Pd_1Ni_1/C–$NaBH_4$ catalysts have been investigated by chronoamperometry (CA) in a 1.0 M NaOH + 1.0 M C_2H_5OH solution, with an applied potential of −0.5 V (vs Hg/HgO), which is set in the low potential range of the Tafel study. Different from other groups which mainly studied the stability in a short period of testing (i.e. 1800–3600 s) [59,78], our tests are focused on a longer term of 10,000 s. The mass activity–time plots are shown in Fig. 8. The mass activities of all Pd-based catalysts at the end of CA and their corresponding mass activities at −0.5 V in the quasi-steady state linear scan voltammetry curves are summarized in Table 4. To set up an evaluation criterion, we defined survival ratio as the MA after 10,000 s CA test to its corresponding MA (at −0.5 V) in the quasi-steady state linear scan (at 1 mV/s), and the results are also summarized in Table 4. The survival ratio indicates the ratio of active sites that remain the catalytic ability toward ethanol oxidation without being poisoned after the long-term reactivity test. The results clearly show a strong correlation between Pd–Ni contacts and long-term EOR reactivity. As shown in Fig. 8, Pd/C and Pd_4Ni_1/C catalysts, which have no or little Ni, were poisoned so heavily that their MAs dropped to ~0 mA/mg at the end of CA test. On the other hand, the MA of Pd_1Ni_1/C–$NaBH_4$ also dropped to ~0 mA because its less effective contact between Pd and Ni could not efficiently remove the 'poisonous intermediates' at such low applied potential. Therefore, after a long-term test, all the surface Pd active sites are poisoned. The survival ratio of all the nanocapsule-synthesized Pd_xNi_y/C catalysts clearly shows a monotonical increase relationship between the long-term EOR reactivity and Ni concentration, with a value of 2%, 6%, 9%, and 12% for Pd_2Ni_1/C, Pd_1Ni_1/C, Pd_4Ni_5/C, and Pd_2Ni_3/C, respectively. However, it is worth noting that the current density will drop quickly in the first 500 s if the ratio of Pd: Ni is less than 1:1, which is probably caused by the lack of enough Pd active sites. As mentioned above, Ni will block the surface Pd active sites if there is an excessive Ni concentration in the Pd_xNi_y/C catalyst. Therefore, although it could increase its reaction stability, a higher concentration of Ni will reduce the total active sites and lower the overall EOR activity.

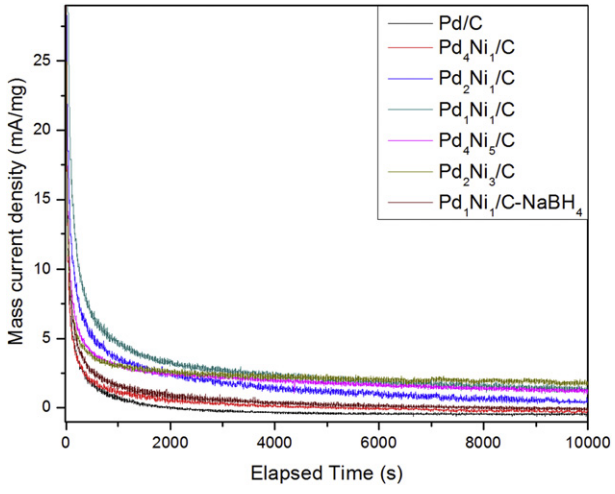

Fig. 8 – Chronoamperometry curves of Pd/C and Pd_xNi_y/C and Pd_1Ni_1/C-$NaBH_4$ catalysts in 1.0 M NaOH + 1.0 M C_2H_5OH, at electrode potential of −0.5 V vs Hg/HgO.

Table 4 – EOR mass activity (MA_1) at the end of 10,000-s chronoamperometry, mass activity (MA_2) at −0.5 V in quasi-steady state LSV (1 mV/s) and survival ratio (MA_1/MA_2) of Pd/C, Pd_xNi_y/C, and Pd_1Ni_1/C catalysts.

	MA_1 after 10000-s CA (mA/mg)	MA_2 at −0.5 V in quasi-steady state LSV (mA/mg)	Survival ratio (MA_1/MA_2)
Pd/C	~0	5.17	–
Pd_4Ni_1/C	~0	7.46	–
Pd_2Ni_1/C	0.37	19.27	2%
Pd_1Ni_1/C	1.33	21.89	6%
Pd_4Ni_5/C	1.29	15.15	9%
Pd_2Ni_3/C	1.71	14.49	12%
Pd_1Ni_1/C-$NaBH_4$	~0	8.08	–

4. Conclusion

In summary, a solution phase-based nanocapsule method has been developed to prepare Pd_xNi_y/C catalysts with small average diameters (2.4–3.2 nm), narrow size distributions (1–6 nm), and large electrochemical surface areas (i.e. 68.0 m^2/

g for Pd_2Ni_1/C). The Pd_xNi_y/C catalysts have demonstrated high reactivity toward EOR in alkaline electrolyte: i.e. the EOR onset potential on Pd_4Ni_5/C is 180 mV more negative than that of Pd/C; the exchange current density of Pd_4Ni_5/C is 33 times higher than that of Pd/C. After a 10,000-s chronoamperometry test at −0.5 V (*vs* Hg/HgO), the mass activity of Pd_2Ni_3/C survived at 1.71 mA/mg, while that of Pd/C had dropped to 0, which implies a better 'detoxification' ability of Pd_xNi_y/C catalysts for maintaining long-term EOR activity. We propose that surface Ni could promote refreshing Pd active sites, thus enhancing the overall ethanol oxidation kinetics. The nanocapsule method is able to not only better control over diameter and size distribution of Pd–Ni particles, but also facilitate the formation of more efficient contacts between Pd and Ni on the catalyst surface, which is the key to improving the EOR activity.

Acknowledgement

We acknowledge the Michigan Tech Start-up Fund D90925 and Research Excellence Fund–Research Seeds (REF-RS) E49236. Acknowledgment is also made to the US National Science Foundation (CBET-1032547) for partial support of this research. We thank Prof. Yan, Yushan for providing TPQPOH anion exchange ionomer. The TGA tests were conducted in ORNL's Center for Nanophase Materials Sciences (CNMS), which was sponsored by the Office of Basic Energy Sciences, U.S. Department of Energy.

REFERENCES

[1] Vielstich W, Lamm A, Gasteiger HA. Handbook of fuel cells: fundamentals, technology, applications, vol. 2. New York: Wiley: Electrocatalysis; 2003.
[2] Basic research needs for the hydrogen economy. U.S. Department of Energy, Office of Basic Science 2004.
[3] Farrell AE, Plevin RJ, Turner BT, Jones AD, O'Hare M, Kammen DM. Ethanol can contribute to energy and environmental goals. Science 2006;311:506–8.
[4] Breaking the Biological Barriers to Cellulosic Ethanol: A Joint Research Agenda A Research Road map Resulting from the Biomass to Bio fuels Workshop Sponsored by the US DOE, December 7–9, Rockville, Maryland 2005.
[5] Breaking the chemical and engineering barriers to lignocellulosic biofuels: next generation hydrocarbon biorefineries, A Joint Research Agenda: A Research Roadmap for making lignocellulosic biofuels a practical reality, Workshop Sponsored by the NSF, ACS and US DOE, June 25-26, Washington, D.C. 2007.
[6] Growth Energy Market Development. http://www.e85refueling.com/index.php.
[7] Lamy C, Belgsir EM, Leger JM. Electrocatalytic oxidation of aliphatic alcohols: application to the direct alcohol fuel cell (DAFC). J Appl Electrochem 2001;31:799–809.
[8] Zhou WJ, Zhou ZH, Song SQ, Li WZ, Sun GQ, Tsiakaras P, et al. Pt based anode catalysts for direct ethanol fuel cells. Appl Catal B 2003;46:273–85.
[9] Zhou WJ, Li WZ, Song SQ, Zhou ZH, Jiang LH, Sun GQ, et al. Bi- and tri-metallic Pt-based anode catalysts for direct ethanol fuel cells. J Power Sources 2004;131:217–23.
[10] Zhao XS, Li WZ, Jiang LH, Zhou WJ, Xin Q, Yi BL, et al. Multi-wall carbon nanotube supported Pt-Sn nanoparticles as an anode catalyst for the direct ethanol fuel cell. Carbon 2004; 42:3263–5.
[11] Lamy C, Rousseau S, Belgsir EM, Coutanceau C, Leger JM. Recent progress in the direct ethanol fuel cell: development of new platinum-tin electrocatalysts. Electrochim Acta 2004; 49:3901–8.
[12] Antolini E. Catalysts for direct ethanol fuel cells. J Power Sources 2007;170:1–12.
[13] Wang Q, Sun GQ, Jiang LH, Xin Q, Sun SG, Jiang YX, et al. Adsorption and oxidation of ethanol on colloid-based Pt/C, PtRu/C and Pt_3Sn/C catalysts: in situ FTIR spectroscopy and on-line DEMS studies. Phys Chem Chem Phys 2007;9:2686–96.
[14] Kowal A, Li M, Shao M, Sasaki K, Vukmirovic MB, Zhang J, et al. Ternary Pt/Rh/SnO2 electrocatalysts for oxidizing ethanol to CO_2. Nat Mater 2009;8:325–30.
[15] Varcoe JR, Slade RCT. Prospects for alkaline anion-exchange membranes in low temperature fuel cells. Fuel Cells 2005;5: 187–200.
[16] Yeager E. Electrocatalysts for O_2 reduction. Electrochim Acta 1984;29:1527–37.
[17] Norskov JK, Rossmeisl J, Logadottir A, Lindqvist L, Kitchin JR, Bligaard T, et al. Origin of the overpotential for oxygen reduction at a fuel-cell cathode. J Phys Chem B 2004;108: 17886–92.
[18] Gasteiger HA, Kocha SS, Sompalli B, Wagner FT. Activity benchmarks and requirements for Pt, Pt-alloy, and non-Pt oxygen reduction catalysts for PEMFCs. Appl Catal B 2005;56: 9–35.
[19] Stamenkovic VR, Fowler B, Mun BS, Wang GF, Ross PN, Lucas CA, et al. Improved oxygen reduction activity on $Pt_3Ni(111)$ via increased surface site availability. Science 2007;315:493–7.
[20] Agel E, Bouet J, Fauvarque JF. Characterization and use of anionic membranes for alkaline fuel cells. J Power Sources 2001;101:267–74.
[21] Yu EH, Scott K. Development of direct methanol alkaline fuel cells using anion exchange membranes. J Power Sources 2004;137:248–56.
[22] Matsuoka K, Iriyama Y, Abe T, Matsuoka M, Ogumi Z. Alkaline direct alcohol fuel cells using an anion exchange membrane. J Power Sources 2005;150:27–31.
[23] Varcoe JR, Slade RCT, Lam How Yee E. An alkaline polymer electrochemical interface: a breakthrough in application of alkaline anion-exchange membranes in fuel cells. Chem Commun; 2006:1428–9.
[24] Park JS, Park SH, Yim SD, Yoon YG, Lee WY, Kim CS. Performance of solid alkaline fuel cells employing anion-exchange membranes. J Power Sources 2008;178:620–6.
[25] Lu SF, Pan J, Huang AB, Zhuang L, Lu JT. Alkaline polymer electrolyte fuel cells completely free from noble metal catalysts. P Natl Acad Sci USA 2008;105:20611–4.
[26] Gu S, Cai R, Luo T, Chen Z, Sun M, Liu Y, et al. A soluble and highly conductive ionomer for high-performance hydroxide exchange membrane fuel cells. Angew Chem Int Ed 2009;48: 6499–502.
[27] Gu S, Cai R, Luo T, Jensen K, Contreras C, Yan YS. Quaternary phosphonium-based polymers as hydroxide exchange membranes. Chemsuschem 2010;3:555–8.
[28] Zhu LD, Zhao TS, Xu JB, Liang ZX. Preparation and chanracterization of carbon -supported sub-monolayer palladium decorated gold nanoparticles for the electro-oxidation of ethanol in alkaline media. J Power Sources 2009; 187:80–4.
[29] Li YS, Zhao TS, Liang ZX. Effect of polymer binders in anode catalyst layer on performance of alkaline direct ethanol fuel cells. J Power Sources 2009;190:223–9.

[30] Spendelow JS, Wieckowski A. Electrocatalysis of oxygen reduction and small alcohol oxidation in alkaline media. Phys Chem Chem Phys 2007;9:2654–75.
[31] Xu CW, Shen PK. Electrochemical oxidation of ethanol on Pt-CeO_2/C catalysts. J Power Sources 2005;142:27–9.
[32] Cui GF, Song SQ, Shen PK, Kowal A, Bianchini C. First-principles considerations on catalytic activity of Pd toward ethanol oxidation. J Phys Chem C 2009;113:15639–42.
[33] Xu JB, Zhao TS, Shen SY, Li YS. Stabilization of the palladium electrocatalyst with alloyed gold for ethanol oxidation. Int J Hydrogen Energy 2010;35:6049–500.
[34] Modibedi RM, Masombuka T, Mathe MK. Carbon supported Pd–Sn and Pd–Ru–Sn nanocatalysts for ethanol electro-oxidation in alkaline medium. Int J Hydrogen Energy 2011;36: 4664–72.
[35] Zhou ZY, Wang Q, Lin JL, Tian N, Sun SG. In situ FTIR spectroscopic studies of electrooxidation of ethanol on Pd electrode in alkaline media. Electrochim Acta 2010;55: 7995–9.
[36] Bambagioni V, Bianchini C, Filippi J, OberhauserIal W, Marchionni A, Vizza F, et al. Ethanol oxidation on electrocatalysts obtained by Spontaneous deposition of palladium onto nickel-zinc Materials. Chemsuschem 2009;2: 99–112.
[37] Bianchini C, Shen PK. Palladium-based electrocatalysts for alcohol oxidation in half cells and in direct alcohol fuel cells. Chem Rev 2009;109:4183–206.
[38] Element Pt & Element Pd. In Periodical Table of Element, www.environmentalchem.com.
[39] Hu FP, Wang Z, Li Y, Li C, Zhang X, Shen PK. Improved performance of Pd electrocatalyst supported on ultrahigh surface area hollow carbon spheres for direct alcohol fuel cells. J Power Sources 2008;177:61–6.
[40] He QG, Chen W, Mukerjee S, Chen SW, Laufek F. Carbon-supported PdM (M = Au and Sn) nanocatalysts for the electrooxidation of ethanol in high pH media. J Power Sources 2009;187:298–304.
[41] Nguyen ST, Law HM, Nguyen HT, Kristian N, Wang SY, Chan SH, et al. Enhancement effect of Ag for Pd/C towards the ethanol electro-oxidation in alkaline media. Appl Catal B 2009;91:507–15.
[42] Demirci UB. Theoretical means for searching bimetallic alloys as anode electrocatalysts for direct liquid-feed fuel cells. J Power Sources 2007;173:11–8.
[43] Sun SH, Murray CB, Weller D, Folks L. Moser, A. Monodisperse FePt nanoparticles and ferromagnetic FePt nanocrystal superlattices. Science 2000;287:1989–92.
[44] Sun SH, Anders S, Thomson T, Baglin JEE, Toney MF, Hamann HF, et al. Controlled synthesis and assembly of FePt nanoparticles. J Phys Chem B 2003;107:5419–25.
[45] Zeng H, Rice PM, Wang SX, Sun SH. Shape-controlled synthesis and shape-induced texture of $MnFe_2O_4$ nanoparticles. J Am Chem Soc 2004;126:11458–9.
[46] Chen M, Kim J, Liu JP, Fan HY, Sun SH. Synthesis of FePt nanocubes and their oriented self-assembly. J Am Chem Soc 2006;128:7132–3.
[47] Hao Z, Jing L, Wang ZL, Liu JP, Sun SH. Bimagnetic core/shell FePt/Fe_3O_4 nanoparticles. Nano Lett 2004;4:187–90.
[48] Luo J, Njoki PN, Lin Y, Wang LY, Zhong CJ. Activity-composition correlation of AuPt alloy nanoparticle catalysts in electrocatalytic reduction of oxygen. Electrochem Commun 2006;8:581–7.
[49] Luo J, Wang LY, Mott D, Njoki PN, Kariuki N, Zhong CJ, et al. Ternary alloy nanoparticles with controllable sizes and composition and electrocatalytic activity. J Mater Chem 2006; 16:1665–73.
[50] Liu ZF, Shamsuzzoha M, Ada ET, Reichert WM, Nikles DE. Synthesis and activation of Pt nanoparticles with controlled size for fuel cell electrocatalysts. J Power Sources 2007;164: 472–80.
[51] Yano H, Kataoka M, Yamashita H, Uchida H, Watanabe M. Oxygen reduction activity of carbon-supported Pt–M (M = V, Ni, Cr, Co, and Fe) alloys prepared by nanocapsule method. Langmuir 2007;23:6438–45.
[52] Li WZ, Chen ZW, Xu LB, Yan Y. A solution-phase synthesis method to highly active Pt–Co/C electrocatalysts for proton exchange membrane fuel cell. J Power Sources 2010;195: 2534–40.
[53] Li WZ, Haldar P. Highly active carbon supported core-shell PtNi@Pt nanoparticles for oxygen reduction reaction. Electrochem Solid-State Lett 2010;13:B47–9.
[54] Li WZ, Haldar P. Supportless PdFe nanorods as highly active electrocatalyst for proton exchange membrane fuel cell. Electrochem Commun 2009;11:1195–8.
[55] Zhang Z, More KL, Sun K, Wu Z, Li W. Preparation and characterization of PdFe nanoleaves as electrocatalysts for oxygen reduction reaction. Chem Mater 2011;23: 1570–7.
[56] Zhang Z, Li M, Wu Z, Li W. Ultra-thin PtFe-nanowires as durable electrocatalysts for fuel cells. Nanotechnology 2011; 22:015602.
[57] Shen SY, Zhao TS, Xu JB, Li YS. Synthesis of PdNi catalysts for the oxidation of ethanol in alkaline direct ethanol fuel cells. J Power Sources 2010;195:1001–6.
[58] Singh RN, Singh A, Anindita. Electrocatalytic activity of binary and ternary composite films of Pd, MWCNT, and Ni for ethanol electro-oxidation in alkaline solutions. Carbon 2009; 47:271–8.
[59] Maiyalagan T, Scott K. Performance of carbon nanofiber supported Pd-Ni catalysts for electro-oxidation of ethanol in alkaline medium. J Power Sources 2010;195:5246–51.
[60] Potentials of Common Reference Electrodes. www.consultrsr.com/resources/ref/refpotls.htm.
[61] Paulus UA, Wokaun A, Scherer GG, Schmidt TJ, Stamenkovic V, Radmilovic V, et al. Oxygen reduction on carbon-supported Pt–Ni and Pt–Co alloy catalysts. J Phys Chem B 2002;106:4181–91.
[62] Jiang L, Hsu A, Chu D, Chen R. Size-dependent activity of palladium nanoparticles for oxygen electroreduction in alkaline solutions. J Electro Chem Soc 2009;156:B643–9.
[63] Medway SL, Lucas CA, Kowal A, Nichols RJ, Johnson D. In situ studies of the oxidation of nickel electrodes in alkaline solution. J Electroanal Chem 2006;587:172–81.
[64] Freitas MBJG. Nickel hydroxide powder for $NiO{\cdot}OH/Ni(OH)_2$ electrodes of the alkaline batteries. J Power Sources 2001;93: 163–73.
[65] Li B, Prakash J. Oxygen reduction reaction on carbon supported palladium-nickel alloys in alkaline media. Electrochem Commun 2009;11:1162–5.
[66] Simoes M, Baranton S, Coutanceau C. Electro-oxidation of glycerol at Pd based nano-catalysts for an application in alkaline fuel cells for chemicals and energy cogeneration. Appl Catal B 2010;93:354–62.
[67] Xiao L, Lu JT, Liu PF, Zhuang L, Yan JW, Hu YG, et al. Proton diffusion determination and dual structure model for nickel hydroxide based on potential step measurements on single spherical beads. J Phys Chem B 2005;109:3860–7.
[68] Wang CB, Gau GY, Gau SJ, Tang CW, Bi JL. Preparation and characterization of nanosized nickel oxide. Catal Lett 2005; 101:241–7.
[69] Bagchi J, Bhattacharya SK. Electrocatalytic activity of binary palladium ruthenium anode catalyst on Ni-support for ethanol alkaline fuel cells. Transit Metal Chem 2007;32: 47–55.
[70] Bagchi J, Bhattacharya SK. Studies of the electrocatalytic activity of binary palladium ruthenium anode catalyst on Ni

support for ethanol alkaline fuel cells. Transit Metal Chem 2008;33:113–20.
[71] Jeong MC, Pyun CH, Yeo IH. Voltammetric studies on the palladium oxides in alkaline media. J Electro Chem Soc 1993; 140:1986–9.
[72] Grden M, Lukaszewski M, Jerkiewicz G, Czerwinski A. Electrochemical behaviour of palladium electrode: oxidation, electrodissolution and ionic adsorption. Electrochim Acta 2008;3:7583–98.
[73] Tripkovic AV, Popovic KD, Lovic JD. The influence of the oxygen-containing species on the electrooxidation of the C_1–C_4 alcohols at some platinum single crystal surfaces in alkaline solution. Electrochim Acta 2001;46:3163–73.
[74] Liang ZX, Zhao TS, Xu JB, Zhu LD. Mechanism study of the ethanol oxidation reaction on palladium in alkaline media. Electrochim Acta 2009;54:2203–8.
[75] Liu HP, Ye JP, Xu CW, Jiang SP, Tong YX. Kinetics of ethanol electrooxidation at Pd electrodeposited on Ti. Electrochem Commun 2007;9:2334–9.
[76] Wang L, Bambagioni V, Bevilacqua M, Bianchini C, Filippi J, Lavacchi A, et al. Sodium borohydride as an additive to enhance the performance of direct ethanol fuel cells. J Power Sources 2010;195:8036–43.
[77] Qin YH, Yang HH, Zhang XS, Li P, Zhou XG, Niu L, et al. Electrophoretic deposition of network-like carbon nanofibers as a palladium catalyst support for ethanol oxidation in alkaline media. Carbon 2010;48:3323–9.
[78] Qin YH, Yang HH, Zhang XS, Li P, Ma CA. Effect of carbon nanofibers microstructure on electrocatalytic activities of Pd electrocatalysts for ethanol oxidation in alkaline medium. Int J Hydrogen Energy 2010;35:7667–74.
[79] Hu FP, Ding FW, Song SQ, Shen PK. Pd electrocatalyst supported on carbonized TiO_2 nanotube for ethanol oxidation. J Power Sources 2006;163:415–9.
[80] Xu CW, Wang H, Shen PK, Jiang SP. Highly ordered Pd nanowire arrays as effective electrocatalysts for ethanol oxidation in direct alcohol fuel cells. Adv Mater 2007;19: 4256–9.
[81] Zheng HT, Li YL, Chen SX, Shen PK. Effect of support on the activity of Pd electrocatalyst for ethanol oxidation. J Power Sources 2006;163:371–5.
[82] Durandkeklikian L, Haq I, Matijevic E. Preparation and characterization of well-defined colloidal nickel compounds. Colloid Surf A 1994;92:267–75.
[83] Parks GA. The isoelectric points of solid oxides, solid hydroxides, and aqueous hydroxo complex systems. Chem Rev 1965;65:177–98.
[84] Moriwaki H, Yoshikawa Y, Morimoto T. Oxide-films on iron and nickel ultrafine particles studied with zero-point of charge measurements. Langmuir 1990;6:847–50.
[85] Lai SCS, Kleijn SEF, Ozturk FTZ, Vellinga VCV, Koning J, Rodriguez P, et al. Effects of electrolyte pH and composition on the ethanol electro-oxidation reaction. Catal Today 2010; 154:92–104.
[86] Vigier F, Coutanceau C, Hahn F, Belgsir EM, Lamy C. On the mechanism of ethanol electro-oxidation on Pt and PtSn catalysts: electrochemical and in situ IR reflectance spectroscopy studies. J Electroanal Chem 2004;563:81–9.